Available online at www.sciencedirect.com
SCIENCE DIRECT®
Catalysis Today 113 (2006) 141–156
CATALYSIS TODAY
www.elsevier.com/locate/cattod

Review

Nucleation, growth and properties of nanoclusters studied by radiation chemistry Application to catalysis

J. Belloni

Laboratoire de Chimie Physique, ELYSE, UMR CNRS/UPS 8000, Université Paris-Sud, 91405 Orsay, France

Available online 19 January 2006

Abstract

For more than three decades, extensive research work has been devoted to the unique properties of clusters. They are made of a small number (or nuclearity) of atoms or molecules only, and therefore constitute a new state of matter, with specific properties. New methods have been developed in physics and chemistry for their synthesis, their direct observation, the study of their properties, and of their crucial role in number of processes, such as phase transition, catalysis, surface phenomena, imaging. Owing to its specific approach, radiation chemistry offered first the opportunity to reveal the existence of nuclearity-dependent properties of clusters. Pulse radiolysis has then proven to be a powerful method to study the mechanisms of cluster formation, induced by irradiation as well as by chemical reduction, and the reactivity in solution or at the interfaces.

Keywords: Metal clusters; Core-shell structure; Alloyed clusters; Redox potential; Growth kinetics; Nucleation mechanism; Catalytic mechanism

Contents

E-mail address: jacqueline.belloni@lcp.u-psud.fr.

0920-5861/$ – see front matter
doi:10.1016/j.cattod.2005.11.082

1. Introduction

Ionizing radiations are known since their discovery, X-rays by Roentgen in 1895 [1] and uranium rays by Becquerel in 1896 [2], to fog the photographic plates, that is to reduce silver ions into atoms, and finally into tiny metal clusters in the emulsion. Progressively, the chemical effects of the absorption of high-energy radiation by liquids were better understood. Particularly, since Fricke's works [3], it was established that the energy is essentially absorbed by the electrons of the solvent which are by far the most abundant. Solutes are only indirectly transformed in a secondary step when they react with the ions, radicals, molecules or excited states generated radiolytically from the solvent. A great deal of comparative studies by X- and γ-rays or electron pulse radiolysis of aqueous solutions of these solutes, used as radical scavengers, converged to the determination of the yields of ions, radicals and molecules produced in water by the radiation:

$$H_2O \rightsquigarrow e_{aq}^-, H_3O^+, H^\bullet, OH^\bullet, H_2, H_2O_2, HO_2^\bullet \quad (1)$$

When noble metal ions were used as scavengers of the reducing radicals, colloids of zerovalent metal were indeed formed. However, the reduction yield presented some irreproducibility and discrepancy with the expected value, or some induction dose was required before the metal colloid appeared [4]. The phenomenon could be related to the well known but unexplained image regression of the latent image in photographic emulsions used for radiation track detection [5]. Moreover, Baxendale et al. [6] observed by pulse radiolysis that silver atoms Ag^0 or charged dimers Ag_2^+, produced by the scavenging of hydrated electrons e_{aq}^- and radicals $H^\bullet$, were easily oxidized by oxygen back to Ag^+. All these facts contradicted the noble character of silver metal [4,5].

According to other results on the radiolysis of Cu^+, also used as a scavenger of reducing species in liquid ammonia [7], no copper clusters were formed and molecular hydrogen was instead produced, as in a subsequent corrosion of copper in its nascent state. We, therefore, explained all these apparent anomalies in concluding that atoms and aggregates of a few atoms presented, in this 'quasi-atomic state', a redox potential much more negative than the bulk metal, making them easily oxidable by oxygen or solvent. The specific properties of clusters were thus due to their highly divided state, constituting a new state of matter, or mesoscopic phase, as later named, between the atom and the crystal [8]. Walker's group [9] determined, by photoionization of transient zerovalent silver species, that their redox potential was lower than that of the bulk metal. Henglein [10] derived from a thermodynamical cycle that the redox potential of silver atoms in water was indeed $E^\circ(Ag^+/Ag^0) = -1.8V_{NHE}$ (2.6 V lower than that of the bulk metal $E^\circ(Ag^+/Ag_{met}) = 0.79V_{NHE}$). This was confirmed by the pulse radiolysis studies showing that atoms are oxidized by a series of moderate oxidizing molecules [11].

Since then, the nucleation of atoms, growth and properties of various metal clusters induced by radiolysis were actively investigated [12–14], as well as the conditions under which ultra-small metal clusters could be stabilized to be applicable to catalysis [12]. The main hypothesis to examine was whether the catalytic efficiency of a cluster could result, not only from its high specific area favoring encounters with the reactants, but also from the specific thermodynamical properties due to its low nuclearity [15]. Various types of catalyzed reactions were studied [12].

The aim of this review is to summarize how the radiation chemistry methods, in the continuous or the pulse regime, are unique tools to determine the mechanism of nucleation and growth of metal clusters and their nuclearity-dependent properties, and how these conclusions can be used to control the synthesis, by irradiation or by chemical methods, particularly in view of applications such as catalysis. The mechanism of some catalytic reactions have also been investigated by the pulse radiolysis method.

2. Radiolytic cluster formation

2.1. Metal ion reduction

The atoms are produced in solution by radiation-induced reduction of the metal ion precursors. The species arising from the radiolysis of water, solvated electrons e_{aq}^- and $H^\bullet$ atoms (1), are indeed the strongest reducing agents. They easily reduce all metal ions, possibly complexed by a ligand, up to the zerovalent state M^0 (Fig. 1). In contrast, sibling radicals which are also formed in radiolysis, such as $OH^\bullet$ in water, are able to oxidize the ions or the atoms into a higher oxidation state. To prevent this oxidation, the solution is added with a scavenger of $OH^\bullet$ radicals such as secondary alcohols (Fig. 1) or formate anions. The secondary radicals formed, α-methyl-hydroxyethyl $H_3C–^\bullet COH–CH_3$ or formyl $^\bullet CO_2^-$ radicals, respectively, are almost as strong reducing species as primary $H^\bullet$ atoms (reaction (1)), also scavenged:

$$H_3C–HCOH–CH_3 + OH^\bullet\,(H^\bullet) \rightarrow H_3C–^\bullet COH–CH_3 + H_2O\,(H_2) \quad (2)$$

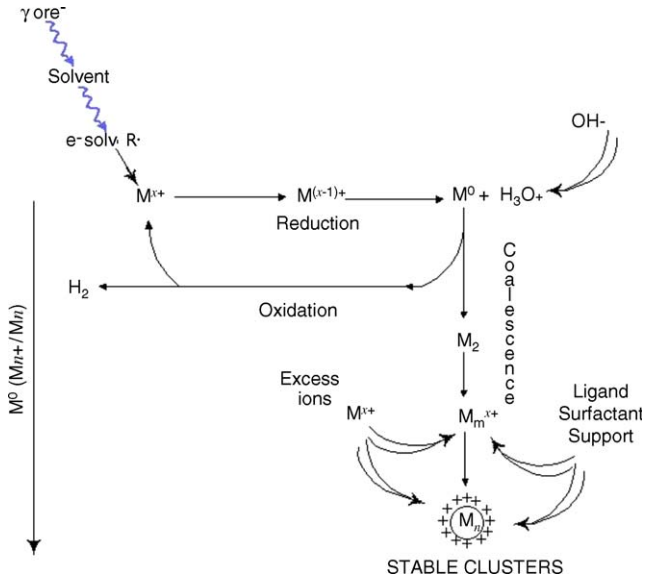

Fig. 1. Scheme of metal ion reduction in solution by ionizing radiation. Alcohol ROH (or formate ion $HCOO^-$) is added in order to scavenge oxidizing radicals. The isolated atoms formed M^0 coalesce into clusters. They adsorb excess ions. They are stabilized by ligands, polymers or supports. The redox potential $E^\circ(M_n^+/M_n)$ increases with the nuclearity. The smallest oligomers may undergo reverse corrosion.

$$HCO_2^- + OH^\bullet\,(H^\bullet) \rightarrow {}^\bullet CO_2^- + H_2O\,(H_2) \quad (3)$$

The solvated electrons and the secondary radicals are able to reduce easily the metal ions, even at room temperature:

$$M^+ + e_{aq}^- \rightarrow M^0 \quad (4)$$

$$M^+ + H_3C{-}{}^\bullet COH{-}CH_3 \rightarrow M^0 + H_3C{-}CO{-}CH_3 + H^+ \quad (5)$$

$$M^+ + {}^\bullet CO_2^- \rightarrow M^0 + CO_2 \quad (6)$$

To prevent oxidation by oxygen or corrosion by protons (produced in (1) and (5)) of the easily oxidable atoms, particularly for non-noble metals [16–19], the solutions are deareated and made slightly basic (Fig. 1). Multivalent ions are also reduced up to the atoms, by multistep processes possibly including disproportionation of lower valency states. Such reduction reactions have been observed directly by pulse radiolysis for a lot of metal ions [20]. Most of their rate constants are known and the reactions are often diffusion controlled.

2.2. Metal atom coalescence

Because the reducing agents, which are generated by the radiation penetrating deeply in the sample, are as randomly distributed as the metal ions in the solution, the atoms are formed with a homogeneous distribution throughout the solution. The binding energy between two metal atoms is stronger than the atom-solvent or atom-ligand bond energy. Therefore, the atoms dimerize when encountering. Then, by a cascade of coalescence processes, M_2 progressively coalesce into growing clusters (Fig. 1):

$$M^0 + M^0 \rightarrow M_2 \quad (7)$$

$$M_m + M_p \rightarrow M_n \quad (8)$$

The bonding between atoms or clusters with unreduced ions is also strong and these association processes are fast:

$$M^0 + M^+ \rightarrow M_2^+ \quad (9)$$

$$M_2^+ + M_2^+ \rightarrow M_4^{2+} \quad (10)$$

$$M_m + M^+ \rightarrow M_{m+1}^+ \quad (11)$$

$$M_{m+x}^{x+} + M_{p+y}^{y+} \rightarrow M_{n+z}^{z+} \quad (12)$$

where m, n and p represent the nuclearities, x, y and z, the number of associated ions. The mechanism has been studied in detail by pulse radiolysis, for example for silver [21]. Optical absorption spectra and reactivity of the transients were determined. Examples of transient spectra of Ag^0 and Ag_2^+ with different ligands in water are given in Fig. 2 [22]. Note that in the pulse regime (at high dose rate), all reducing species are produced and scavenged within a short time (reactions (1)–(6)),

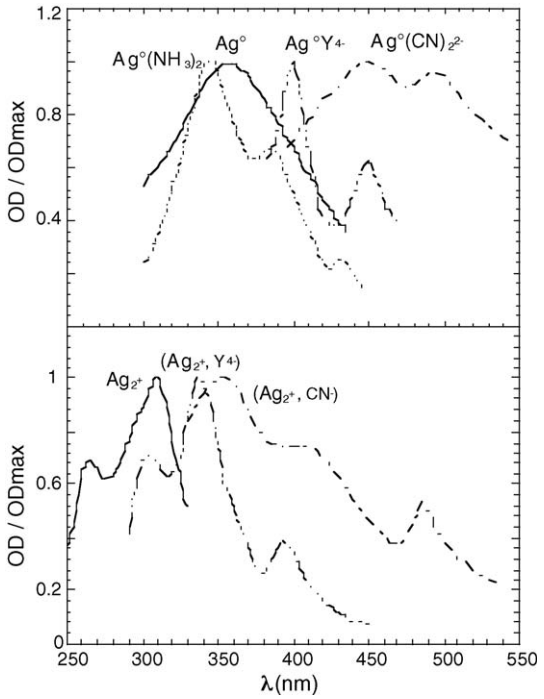

Fig. 2. Optical absorption spectra of Ag^0L and Ag_2^+L (L: CN^-, NH_3, or EDTA anion = Y^{4-}), as obtained by pulse radiolysis at nanosecond range of a solution containing Ag^IL, compared with the spectra of the corresponding species without ligand in water [22].

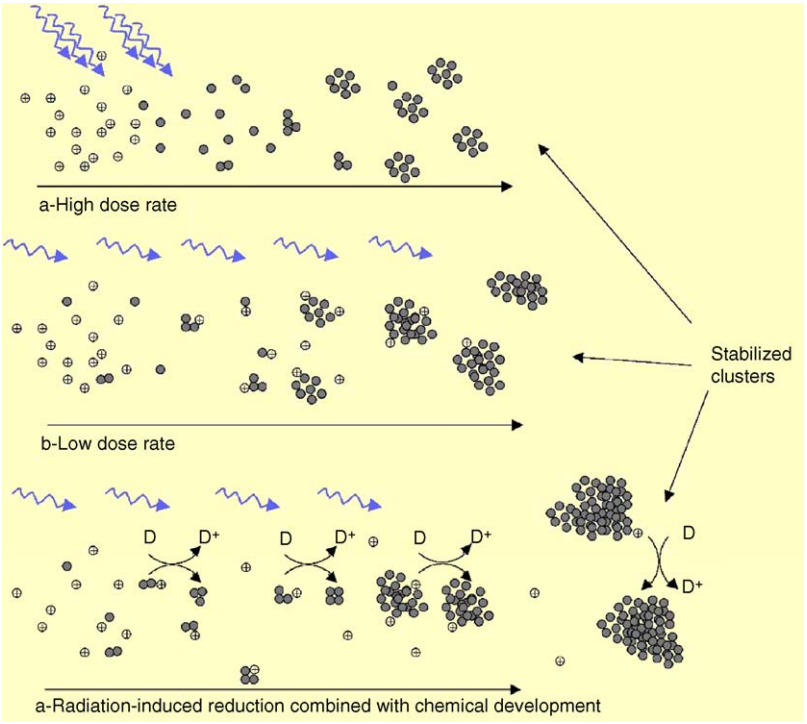

Fig. 3. Nucleation and growth of clusters generated by radiolytic radicals at high (a) and low (b) dose rates, without or with an electron donor D (c). The arrows symbolize the increasing time. The stabilizing effect of the polymer prevents exclusively coalescence beyond a certain limit of nuclearity, but does not prevent successive ion and electron transfers (from the radicals at low dose rate and from the donor), which let develop the cluster up to much larger sizes [23].

followed by the steps of coalescence of atoms separately created (reactions (7)–(12); Fig. 3a) [23]. In contrast, in the continuous irradiation regime (at low dose rate), the association of M^+ ions with atoms, as in the charged dimer M_2^+ and clusters M_{n+1}^+ (reactions (9) and (11)), and the coalescence processes (reactions (10) and (12)) are faster than the production rate of the reducing radicals (reactions (1)–(3)). Therefore, the reduction of M^+ ions occurs mostly in situ on clusters already formed M_{n+1}^+ (reactions (4′)–(6′)):

$$M_{n+1}^+ + e_{aq}^- \rightarrow M_{n+1} \quad (4')$$

$$M_{n+1}^+ + H_3C{-}{}^{\bullet}COH{-}CH_3 \rightarrow M_{n+1} + H_3C{-}CO{-}CH_3 + H^+ \quad (5')$$

$$M_{n+1}^+ + {}^{\bullet}CO_2^- \rightarrow M_{n+1} + CO_2 \quad (6')$$

As a consequence, the new atoms formed are not isolated but contribute to let grow a smaller amount of preformed nuclei (Fig. 3b). In fact, the final nuclearity and radius of clusters are found to be systematically larger by steady than by pulse irradiation. Likewise, the redox potential of chemical agents (electron donor D) other than solvated electrons is generally not negative enough to reduce isolated metal ions to atoms (Section 3). Thus, they essentially reduce ions adsorbed on the nuclei generated by radiolysis, a development process which results in still larger clusters (Fig. 3c) [23].

2.3. Cluster stabilization

The radiolytic method of cluster synthesis can be used in various environments. The control of the final size depends on the limitation applied to the coalescence beyond a certain nuclearity.

For free clusters such as nanocolloids in solution, the coalescence may be limited by a polymeric molecule acting as a cluster stabilizer. Functional groups with high affinity for the metal ensure the anchoring of the molecule at the cluster surface while the polymeric chain protects the cluster from coalescing with the next one, and thus inhibits at an early stage further coalescence through electrostatic repulsion or steric hindrance [12]. The final size of metal clusters depends on the metal, decreases when the initial polymer/ion ratio increases and lies in the nanometric range (1–20 nm). The polymer should not chemically reduce the ions fixed on the clusters so as to prevent their growth (Section 3). Poly(vinyl alcohol) (PVA), for example, fulfills these criteria (Fig. 4). The radiolytic method was used for the synthesis of a great number of noble and non-noble metal nanocolloids in various solvents, water [12], liquid ammonia [15] and alcohols [24]. They present the specific optical spectrum due to the surface plasmon band according to Mie model [25] (in water: λ_{max} = 380 nm for Ag_n, 520 nm for Au_n, 570 nm for Cu_n and the maximum wavelength is in the UV for the others [23]). For such small sizes, no light scattering is observed. Cobalt or nickel clusters are ferromagnetic. As a consequence of the initial homogeneous distribution of atoms, the size distribution of clusters is remarkably narrow,

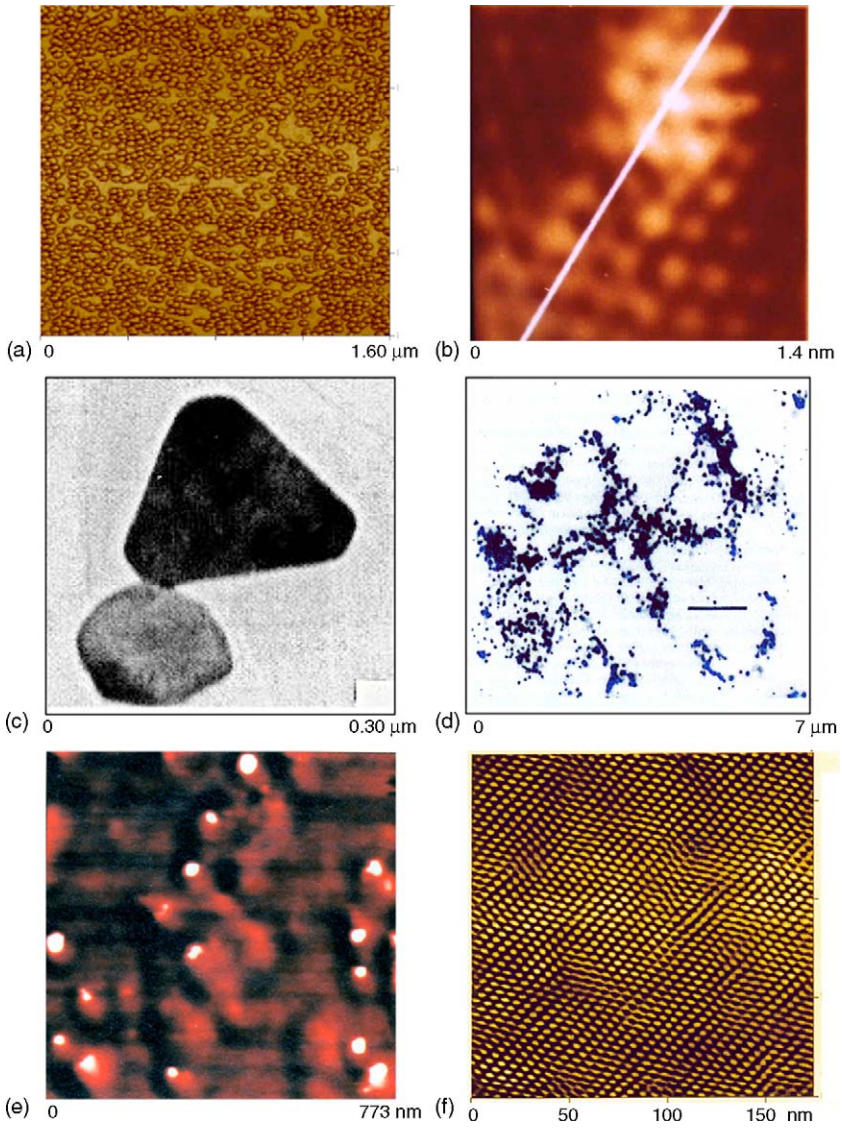

Fig. 4. Radiation-induced metal clusters. (a) Silver nanoclusters stabilized by PVA, $n = 10^5$ (10 nm). (b) STM imaging of a single cluster of the blue sol of silver oligomers Ag_7^{3+} formed by γ-irradiation (0.10 kGy). Ag_2SO_4 10^{-3} mol l^{-1}, PA, 75 days aged, $n = 4$ [28]. (c) Clusters Ag_n partially reduced by irradiation then chemically developed by EDTA, $n = 10^8$ (100 nm large and 15 nm thick) [53]. (d) TEM bright-field image of Ni_n, PVA clusters (20 nm). Scale bar: 500 nm [16]. (e) Phase imaging in tapping mode AFM of gold clusters (10 nm), showing the discrimination with the polymer PVA [27]. (f) Two-dimensional layer of gold clusters (PVA) with remarkable homodisperse size (5 nm) [26].

as shown in Fig. 4a and d–f. They can even arrange in a two-dimensional array when the droplet of the nanometric colloidal sol is dried on the HOPG surface (Fig. 4f) [26]. Phase imaging in tapping mode AFM is a powerful tool for the characterization of clusters stabilized by polymer matrices as shown for the first time in observing silver and gold samples [27]. In Fig. 4e, the phase detection helps to discriminate between amorphous polymer and silver clusters.

In the absence of an added radical scavenger, the polymer PVA, whose alcohol groups are also able to scavenge $OH^\bullet$ and $H^\bullet$, can be cross-linked under irradiation during the simultaneous reduction of metal ions (silver, palladium, nickel, ...) [12]. Finally, after drying, the clusters formed are trapped in a thin polymeric film, which presents the specific optical absorption band of the metal nanoparticles. In the case of nickel, the film is ferromagnetic.

Another polymer, sodium polyacrylate (PA), displayed the property at low dose to stop the coalescence at only a few atoms. Such oligomers of silver Ag_7^{3+} (Fig. 4d) [28,29] or platinum Pt_{5-7} [30] were observed by STM and by their optical absorption spectrum (band maximum at 800 nm for blue silver [31] and 540 nm for pink nickel oligomers [32]). It was concluded that the metal–acrylate interaction is comparable to a strong ligandation. The silver or platinum oligomers stabilized by PA are long-lived even in air, but nickel-PA oligomers are spontaneously oxidized by water within 1 day.

Some ligands, such as CN^- for gold or silver clusters, are also able to stabilize, without added polymer, small sized particles, probably because they are strongly linked to the cluster, thus protecting them from coalescence by electrostatic repulsion. However, the redox potential of these clusters is more negative than without CN^- and they are extremely fragile

to oxygen [33]. In contrast, air-stable molecular carbonyl clusters of various metals [12,34–36], such as Chini clusters $[Pt_3(CO)_6]_m^{2}$ with $m = 3$–10, can be easily obtained by radiation-induced reduction of metal ions under CO atmosphere. The synthesis is selective and m is controlled by adjusting the dose (high doses yielding low m values).

2.4. Supported nanoclusters

One of the important applications of metal clusters is to be used as catalysts on solid supports. When the ion solution is in contact with the support, the metal ions diffuse in the pores and adsorb at the surface. The ionizing radiation penetrates throughout the support and forms nascent atoms in situ, which are strongly fixed at the surface. Because they are generated at room temperature, they do not diffuse much, so that the sintering is low, and quite small clusters can be produced without stabilizing polymer. As the method does not necessitate heating, it also prevents thermal destruction of polymeric supports.

The coalescence of atoms into clusters is thus limited by generating the atoms inside confined volumes of microheterogeneous structures of porous materials, such as zeolites [37,38], microorganized systems [39,40], alumino–silica gels [12,41], colloidal oxides such as TiO_2 [42] or polymeric membranes [43,44]. The radiolytic synthesis was also successfully used to produce metal clusters supported on various micropowered oxides [15,18,19,45] or on carbon [12,35,46] (an alternative method consists in first preparing, by irradiation in solution, nanometric metal clusters which are then deposited on the support by filtration or simple contact). Due to the high specific area of the supports, concentrated solutions of ions are used. Depending on the support surface charge and the metal ion charge, respectively, the preliminary ion adsorption, and the subsequent location of clusters may be restricted to the outer surface of the support particle or may occur deeply in the pores [37,44]. For example, the cationic precursors are included deeply into the cavities of a Nafion® polymeric membrane by ion-exchange before irradiation. After absorption at room temperature of the radiation which penetrates the membrane and the solution in pores, the process of cluster formation is the same as in reactions (1)–(12). However, the observation of the coalescence process by pulse radiolysis has shown that the diffusion of species through channels connecting the pores is much slower than in free water (by a factor of 10^4–10^5 for silver). Similarly, platinum or nickel clusters can be generated inside Nafion® membrane cavities. Then, the clusters are trapped in the microvolumes, where they are still accessible to reactants for catalysis [44].

3. Nuclearity-dependent redox potential of clusters

The most important changes in cluster reactivity occur, as for other properties, at low nuclearity. However, due to the spontaneous coalescence, the small oligomers are generally short-lived and observable only by pulse radiolysis and time-resolved detection in the course of their coalescence. Likewise, the determination of their reactions is accessible only by kinetics methods studying the influence on their usual coalescence processes of a possible competitive reaction with an added reactant of known redox potential. Depending on the reactant, metal clusters M_{n+1}^{+} may behave as electron donors or electron acceptors. In the first case, they are oxidized into the ions (some examples, such as spontaneous oxidation in air, were given above).

3.1. Nuclearity-dependent cluster potential

In the case, clusters are electron acceptors, the electron reduces the metal ion fixed on the cluster and the cluster nuclearity is incremented by one unit. Experimentally [47,48], we observe at which step n of the coalescence reaction cascade (7)–(12), a reaction of electron transfer occurring from a donor D to the cluster M_n^{+} could compete with (12). Indeed n is known from the measured coalescence rate constant and the time elapsed from the start of coalescence when atoms have been generated by the pulse. The donor D (such as reduced forms of sulfonato-propyl viologen, methyl viologen or naphtazarin) is produced by the same pulse as the atoms M^0. The process kinetics is observed by the evolution of the couple D^+/D optical absorption [47,48] (Fig. 5).

The transfer requires that $E^\circ(M_n^{+}/M_n)$, which increases with n during the spontaneous coalescence, becomes higher than the reference potential $E^\circ(D^+/D)$. The redox potential of the reference donor, thus creates a threshold for n, that is a critical nuclearity n_c. As far as $n < n_c$, it is observed indeed that the coalescence (reactions (1)–(12)) occurs as in the absence of D and that the absorbance of D remains constant because ions could not be reduced except by radiolytic species (Fig. 5). However, when $n \geq n_c$, D starts to decay due to an electron transfer to M_n^{+}:

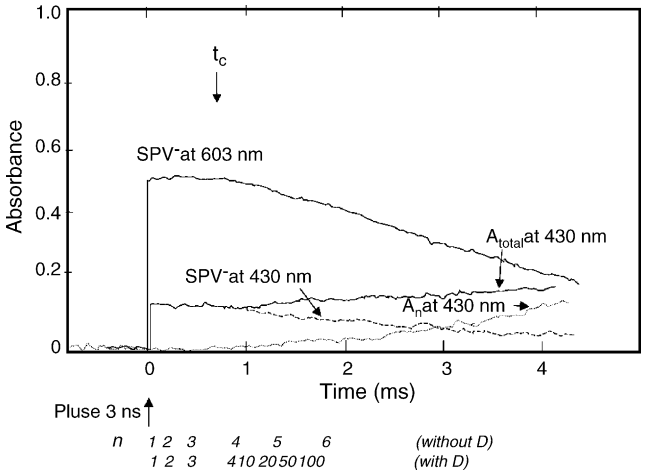

Fig. 5. Kinetic signals of the transient optical absorption of the electron donor decay (reduced form of sulfonato-propyl viologen at 603 nm, D = $SPV^{\bullet-}$) after a critical time t_c, and of the corresponding autocatalytic growth of silver clusters (at 430 nm). Single electron pulse of 3 ns in a mixed solution of silver ions and SPV. Below the time abscissae, the nuclearities are indicated when they appear successively, without or with the donor D [47].

$$M_n^+ + D \rightarrow M_n + D^+ \quad (13)$$

$$M_n + M^+ \rightarrow M_{n+1}^+ \quad (14)$$

$$M_{n+1}^+ + D \rightarrow M_{n+1} + D^+ \quad (15)$$

Simultaneously, the clusters grow autocatalytically by successive reduction of adsorbed ions into atoms (13) and (15), and addition of a supplementary ion (14). Once formed, a supercritical cluster behaves indeed as a growth nucleus. The cascade of alternate reactions (13) and (14) makes its redox potential more and more favorable to the transfer, so that an autocatalytic growth is observed up to the total consumption of D or M^+. The study of the influence of the initial concentration ratio $[D]/[M_1]$ also confirms the mechanism: at given dose per pulse (or given initial reduction amount ($[D] + [M_1]$), and increasing ratio $[D]/[M_1]$, less nuclei M_{nc} are formed by radiolysis and each of them is developed to larger sizes [47]. The transfer rate constant k_{13} and the critical nuclearity n_c are derived from the fitting between the kinetics of the experimental donor decay and numerical simulations [47,48]. In the example of Fig. 5, the transfer starts for Ag_5^+ ($n_c = 4$). The redox potential of M_{nc} is just above that of the reference donor.

By changing the reference potential in a series of redox monitors (reduced forms of sulfonato-propyl viologen, methyl viologen or naphtazarin), the dependence of the cluster potential on the nuclearity was obtained, for example for silver or copper clusters. The potential $E^\circ(Ag_n^+/Ag_n)_{aq}$ in water increases with n as shown in Fig. 6 [48]. The asymptotical value of the redox potential is reached at the nuclearity around $n = 500$ (radius ≈ 1.25 nm). Since the Fermi potential of the normal hydrogen electrode is at 4.5 eV, a comparison can be also made between the nuclearity effects on $E^\circ(Ag_n^+/Ag_n)_{aq}$ and on the ionization potentials IP_g (Ag_n) of bare silver clusters in the gas phase [49]. It is obvious from this figure that the variations of E° and IP_g do exhibit opposite trends versus n, for the solution and the gas phase, respectively. The origin lies indeed in the solvation free energy of the cation Ag_n^+ which in water assists the ionization of Ag_n. The difference between ionization potentials of bare and solvated clusters decreases with increasing n and corresponds fairly well to the solvation free energy of the cation Ag_n^+ deduced from the Born model [50]. Note that the nuclearity of the silver cluster corresponding to the same potential $-0.41 V_{NHE}$ is $n_c = 6 \pm 1$ in the presence of the ligand CN^- [51], instead of $n_c = 4$ for the aquo complex. An increase of $E^\circ(Cu_n^+/Cu_n)$ for copper was found similar to that of silver with increasing the cluster nuclearity n [52]. More generally, due to the high value of the sublimation energy of metals, the redox potential of any metal atom $E^\circ(M^+/M^0)$ is expected to be quite negative, and the oligomer potential to be lower than that of the bulk metal.

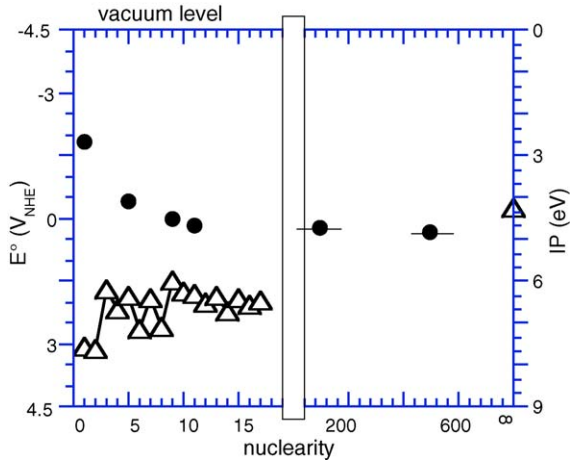

Fig. 6. Size-dependence of the redox potential of silver clusters in water (●, left ordinate scale) [48,50] and the ionization potential of silver clusters in the gas phase (Δ) [49]. The redox potentials refer to the normal hydrogen electrode whose Fermi potential is at 4.5 eV.

3.2. Growth by development mechanism

The mechanism may be exploited to let grow, by radiolytic reduction combined with chemical reduction under controlled conditions, a small number of nuclei developed up to large sizes [47] (Fig. 3c). The homogeneous size of the clusters acting as seeds is ensured by the radiation-induced synthesis. The enlargement during the growth is fixed by the ratio between the concentrations of the supercritical clusters and of the excess ions, which are chemically reduced by the reductant exclusively when adsorbed at the surface of the seeds [47]. In the case of EDTA silver complexes, nanosized silver clusters (10–15 nm) are produced first by γ-irradiation. Then, as a slow post-effect, the growth by EDTA chemical reduction of adsorbed ions is favored at the 1 1 1 surface, and produces triangular particles 15 nm thick and 100–150 nm large [53] (Fig. 4c). Similarly, radiation-induced gold clusters grow slowly in a post-effect through chemical reduction in situ of adsorbed ions by monocharged methyl viologen [54] or 2-propanol [55]. The lower the dose or the number of nuclei, the larger the final size of the cubic crystallites nicely homodisperse. Depending on the respective parts of both types of reduction, the size may range from 10 to 500 nm [55]. Nickel clusters, prepared by irradiation and stabilized by PA, act as catalytic nuclei for the reduction of adsorbed Ni^{2+} by hypophosphite ions up to large and ferromagnetic particles, while free Ni^{2+} ions, with much lower potential than adsorbed ions, cannot be directly reduced [32].

Likewise, in chemical reduction processes not induced by irradiation, most of nucleation and growth mechanisms are controlled by the electron donor potential and the nuclearity-dependence of the cluster redox potential [23]. Note that the redox potential of ions adsorbed on supports is also more positive (as when adsorbed on clusters on the same metal) than for free ions in solutions. Therefore, a moderate reducing agent, not strong enough (in contrast with e_{aq}^-) to reduce free solvated metal ions into the zerovalent state, is able to reduce exclusively the adsorbed ions and to achieve the surface growth of the metal clusters by reactions (13)–(15), such as in the classical formation process of silver mirror on glass. This demonstrates the important role that adsorption on walls could play in the

chemical reduction. This autocatalytic surface-controlled growth can be compared, when the direct reduction of free ions is thermodynamically excluded, to a development (Fig. 3c), and results in larger clusters than in radiation-induced nanocolloidal solutions (Fig. 3a and b).

4. Bi and multimetallic clusters

Composite clusters are of prominent interest for catalysis of chemical reactions. It seems particularly important that atoms of different metals can be located at the cluster surface as in an alloy. The control of the conditions for the synthesis of composite metal clusters containing M and M′ in variable proportions, with either an alloyed or a core/shell structure, is therefore crucial. Actually, when a mixed solution of two ionic precursors M^+ and M'^+ is irradiated, both situations of alloyed or, more often, bilayered cluster formation were encountered without clear prediction [12]. Moreover, the characterization of the structure of a composite nanocluster is particularly difficult due to its small size. It is scarcely achieved in the literature. But the information can be given for some systems by the study of the influence of the increasing irradiation dose on the progressive ion reduction in a mixed solution.

4.1. Core-shell clusters

In many cases, even though M^+ and M'^+ have generally equal probabilities to be reduced by radiolytic radicals (reactions (4)–(6) and (4′)–(6′)), a further electron transfer from the less noble atoms (for example, M′) to the more noble ions M^+ systematically favors first the reduction into M.

$$M'^0 + M^+ \rightarrow (M\,M')^+ \rightarrow M^0 + M'^+ \quad (16)$$

$$(M_m M'_n)^{x+} + M^+ \rightarrow (M_{m+1} M'_n)^{(x+1)+} \rightarrow (M_{m+1} M'_{n-1})^{x+} + M'^+ \quad (17)$$

If the ionic precursors are plurivalent, an electron transfer is possible as well between the intermediate low valencies of both metals, so increasing the probability of segregation. The less noble metal ions act as an electron relay towards the noble ions. Thus, monometallic clusters M_n are formed first. Then, when M^+ ions are exhausted, M'^+ ions are reduced afterwards at the surface of M_n. The final result is a core-shell cluster where the more noble metal M is coated by the other one M′.

Fig. 7 top presents the evolution, at increasing γ-irradiation dose, of the optical absorption spectra of mixed equimolar solutions of $KAuCl_4$ and Ag_2SO_4 in the presence of PVA at the dose rate of 3.8 kGy h^{-1} [56]. At first, the optical absorption spectrum is identical to the surface plasmon band of pure gold clusters with a maximum at 520 nm up to a dose of 2 kGy. Local X microanalysis of clusters at this partial reduction step clearly indicates that gold is predominant in the particles. At higher doses, the absorption intensity still increases but the colloidal solution turns from pink to deep yellow and the single absorption maximum is progressively shifted to 440 nm (to be compared with that of pure silver clusters at around 400 nm). The shift of the surface plasmon spectrum indicates that the cluster composition changes with dose from almost pure gold clusters to Au_{core}/Ag_{shell} clusters of gold coated with a silver layer of increasing thickness. Although silver and gold crystallize with the same fcc lattice and very close a_0 parameters (Ag: 0.4086 nm and Au: 0.4078 nm), the segregation is not prevented, because the reduction process is controlled by the respective redox potentials. The initially reduced silver atoms have been reoxidized in a further step through electron transfer to gold ions (reaction (16)) as far as gold ions are not totally reduced (Fig. 7 top). Then, the silver reduction occurs at the surface of gold clusters, just formed, which adsorbed most of excess silver ions. The final band intensity of 50/50 silver-coated gold clusters corresponds to a mean extinction coefficient per Ag or Au atom of $\varepsilon_{440} = 4700\ l\ mol^{-1}\ cm^{-1}$ (Fig. 7 top). The subcolloidal solutions are then stable with time and their spectrum does not change, even in the presence of air.

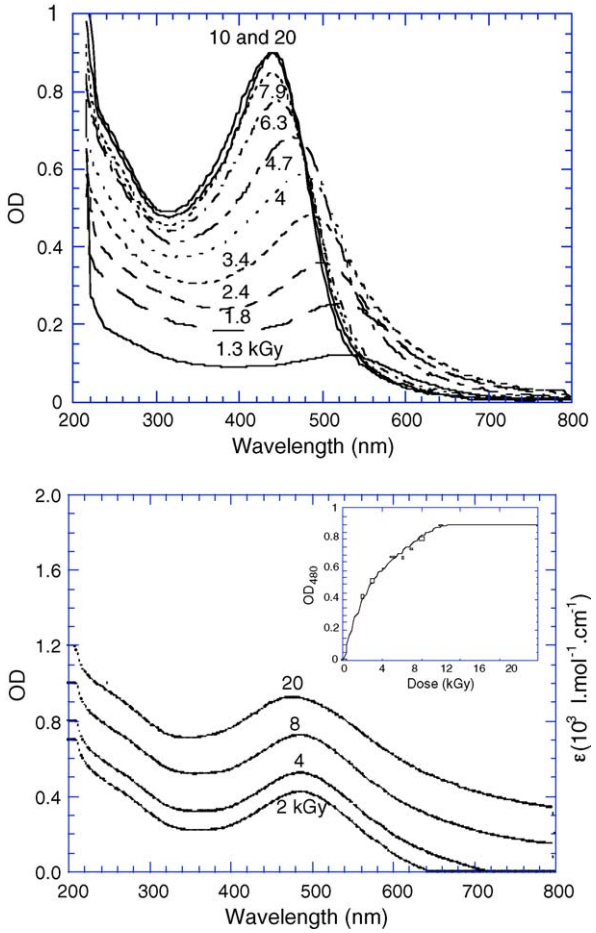

Fig. 7. Evolution with increasing γ-dose of the absorption spectra of a mixed solution. $[Au^{III}] = [Ag^I] = 5 \times 10^{-4}$ mol l^{-1}, [PVA] = 0.1 mol l^{-1}, [2-propanol] = 0.2 mol l^{-1}, pH 10. Optical path 2 mm. *Top:* Dose rate of 3.8 kGy h^{-1}. *Bottom:* Dose rate of 35 kGy h^{-1}. *Inset:* Evolution with increasing dose of the absorbance at λ = 480 nm [56].

In contrast, if the ionic precursors are gold and silver cyanide, zerovalent silver is now favored during the reduction and is formed first because gold behaves as the less noble metal,

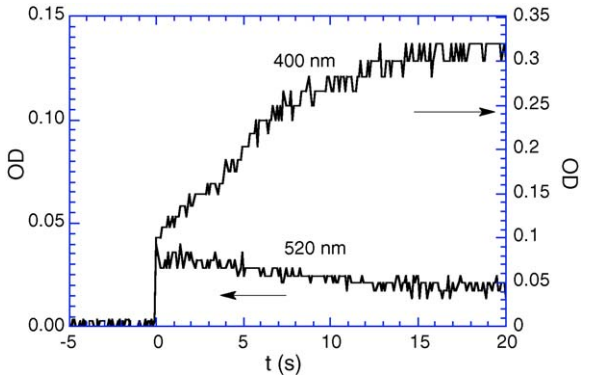

Fig. 8. Correlated signals at 400 nm (right ordinate scale) and 520 nm (left ordinate scale) with a single pulse in equimolar mixed solution of gold and silver cyanide, $Ag(CN)_2^-$ and $Au(CN)_2^-$, in the presence of 2-propanol [51].

according to the respective electrode potentials in the presence of cyanide. The silver cluster band is observed first, which is then, after gold reduction, eventually shifted to the red, thus suggesting the formation of the bilayered Ag_{core}/Au_{shell} particles [51]. A pulse radiolysis study of the same mixed system of monovalent cyano-silver and gold ions provided the first time-resolved observation of an intermetallic displacement as in reactions ((16) and (17)) [51] (Fig. 8). At short time, both types of metal atoms are formed and excess ions not reduced remain, but then, in the time-range of seconds, the intensity of the plasmon band of silver clusters increases slowly while that of gold decays, due to the electron transfer from gold atoms to cyano-silver ions. Other examples of bimetallic core-shell clusters are given on Table 1. They can be prepared also by irradiation in a two-step process, production of the core in the noble metal solution, then core-coating by reduction of the added ions of the second metal.

Table 1
Multimetallic clusters

Synthesis and irradiation conditions		Particle structure [Ref.]
Mixed salts or (cluster, salt) couple[a]	Irradiation source dose rate (kGy h^{-1})	
Ag_n, $Au(CN)_2^-$	γ, 0.9	Ag/Au, core-shell [71]
$Ag(CN)_2^-$, $Au(CN)_2^-$	γ, 35	Ag/Au, core-shell [56]
$Ag(CN)_2^-$, $Au(CN)_2^-$	EB, 7.9×10^3	AgAu, alloy [56]
Ag^+, $AuCl_4^-$	γ, 3.8	Au/Ag, core-shell [56]
Ag^+, $AuCl_4^-$	γ, 35; EB, 7.9×10^3	AgAu, alloy [56]
Ag^+, Cd^{2+}	γ, 0.87	Ag/Cd, core-shell [72]
Ag_n, Cu^{2+}	γ, 0.87	Ag/Cu, core-shell [48,73]
Ag_n, In^{3+}	γ,	Ag/In, core-shell [74]
Ag^+, Pd^{2+}	γ, 35	AgPd, alloy [57]
Pd_n, $Ag(CN)_2^-$	γ, 0.87	Pd/Ag, core-shell [75]
Ag^+, $PtCl_6^{2-}$	γ, 30	AgPt, alloy [76]
$AuCl_4^-$, Pd^{2+} ,	γ, 6	Au/Pd, core-shell [59,77]
$AuCl_4^-$, Pd^{2+} ,	EB, 7.9×10^3	AuPd, alloy [59]
$AuCl_4^-$, $PtCl_6^{2-}$,	EB, 7.9×10^3; γ, 0.5–40	Au/Pt, core-shell [60]
$Au(CN)_2^-$, $PtCl_6^{2-}$	EB, 7.9×10^3; γ, 0.5–40	Pt/Au, core-shell [61]
Au_n, Pb^{2+}	γ, 0.4, 0.87	Au/Pb, core-shell [78]
Au_n, Pb^{2+}, Cd^{2+}	γ, 0.87	Au/Pb/Cd tri-layer [79]
Au_n, Cd^{2+}	γ, 0.4	Au/Cd, core-shell [79]
Au_n, Tl^+	γ, 0.4	Au/Tl, core-shell [79]
Au_n, Sn^{2+}	γ, 0.4	AuSn, alloy [80]
Cu^{2+}, Cd^{2+}	γ, 0.42, 0.48	CuCd, alloy [81]
Cu^{2+}, Pd^{2+}	γ, 30	CuPd, alloy [16]

[a] The ions of M′ are introduced in a second step after the formation of the cluster M_n, and are then reduced by γ-irradiation.

4.2. Alloyed clusters

In some other cases, the intermetal electron transfer does not occur even during hour-long irradiation [16]. The initial reduction reactions ((4)–(6)) are followed by mixed coalescence:

$$M' + M \rightarrow (M\,M') \tag{18}$$

$$(M\,M') + M \rightarrow (M_2\,M') \tag{19}$$

and association of atoms and clusters with ions and reduction in situ as in reactions (4′)–(6′):

$$(M_m\,M'_n)^{x+} + M^+ \rightarrow (M_{m+1}\,M'_n)^{(x+1)+} \tag{20}$$

$$(M_{m+1}\,M'_n)^{(x+1)+} + e^-_{aq}(\text{or R}) \rightarrow (M_{m+1}\,M'_n)^{x+}(\text{or} + R^+) \tag{21}$$

Then alternate association (20) and reduction reactions (21) progressively build bimetallic alloyed clusters according to the statistics of encounters, therefore to the relative initial ion concentration. For example, the sol formed, when mixed $CuSO_4$ and $PdCl_2$ solution (PVA) is γ-irradiated, is dark green (instead of pink for Cu or brown for Pd monometallic clusters) [16]. The structure of the clusters, as analyzed by electron diffraction, is clearly that of solid solutions. Moreover, superlattice reflections imply ordered atomic arrangements. Superlattices corresponding to Cu_3Pd fcc structures are observed for Cu^{2+}/Pd^{2+} 90/10 mixtures and CuPd for Cu^{2+}/Pd^{2+} 50/50 solutions. Similar superlattices Ni_3Pt (in $Ni^{2+}/PtCl_4^-$ 90/10) were found [16]. Nickel is also easily alloyed with ruthenium. Although monometallic iron clusters are unstable in the irradiated solution, ferromagnetic alloyed Cu–Fe clusters may be formed in the mixed Cu^{2+}/Fe^{3+} solution. Intimately alloyed nanoclusters of Ag_x–Pd_{1-x} are obtained at the dose rate of 35 kGy h^{-1} at any x value and the superlattice of Ag_3Pd was observed. The maximum wavelength of the plasmon surface optical band depends on x [57] as in Mie model [25]. Other examples of alloyed clusters are given on Table 1.

4.3. Dose rate effects

In fact, the possible formation of an alloyed or a core-shell cluster depends on the kinetic competition between, on one hand, the irreversible release of the ions of the less noble metal displaced by the excess ions of the more noble metal after electron transfer (reactions (16) and (17)), and on the other hand, the radiation-induced reduction of both metal ions (reaction (21)). This competition depends therefore on the

metals and also on the dose rate. The pulse radiolysis study of the mixture of cyano-silver and gold complexed ions (Fig. 8) suggested that the electron transfer may be rather slow, and that a very fast and total reduction (out of redox thermodynamics equilibrium) by the means of a powerful and more sudden irradiation could prevent the electron transfer and produce alloyed clusters (Fig. 9). The sudden and complete reduction of ions of both types is thus followed by a coalescence of atoms M and M′ into alloyed clusters. Some ordered arrangements of atoms may be obtained.

Indeed such a decisive effect of the dose rate has been demonstrated [56]. When the mixed solution of cyano-gold and silver ions is irradiated at high dose rate with an electron beam, allowing the sudden and complete reduction of all the ions prior to the electron transfer, the clusters are alloyed [56]. In contrast with the results at the dose rate of 3.8 kGy h^{-1} (Fig. 7 top), when the same solutions of $KAuCl_4$ and Ag_2SO_4 are γ-irradiated at the higher dose rate of 35 kGy h^{-1}, the shape of the spectrum does not change with dose while the intensity progressively increases (Fig. 7 bottom). The same evolution with dose is also found when the sample is irradiated by an electron beam at the dose rate of 7.9×10^3 kGy h^{-1}. The new plasmon band for the 0.50/0.50 alloy is now centered at 480 nm, an intermediate value between 400 nm (Ag_n) and 520 nm (Au_n). The maximum absorbance at complete reduction corresponds to an extinction coefficient of $\varepsilon_{440} = 4500\ l\ mol^{-1}\ cm^{-1}$ per metal atom. This identical spectrum shape at any dose therefore testifies in the existence of the same

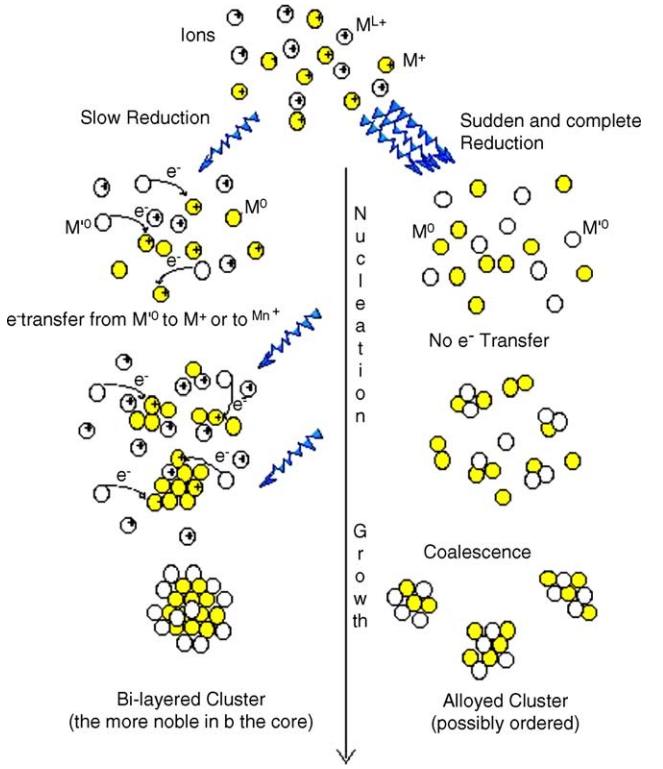

Fig. 9. Scheme of the influence of the dose rate on the competition between the inter-metal electron transfer and the coalescence processes during the radiolytic reduction of mixed metal ion solutions. High dose rates favor alloying whereas low dose rates favor core-shell segregation of the metals in the clusters [23].

strong interaction between the two metals, which are alloyed in a constant proportion from the lowest doses, and consequently identical to that of the ionic precursors. A comparative study by local X-analysis along the diameter of these clusters confirmed that the core-shell or alloyed structure depended indeed on the dose rate [58]. The same evolution with the dose has been studied for various values of the x fraction of Au ions in the initial solution at the high dose rate, and various alloyed $Ag_{1-x}Au_x$ clusters were obtained. The maximum wavelength λ_{max} and the extinction coefficient ε_{max} of the alloy depend on x [56], according to Mie model [25]. Superlattice of Au_3Ag has been detected in an irradiated Au^{III}/Ag^{I}/PA 0.68/0.32 sample. Moreover, the TEM images obtained from alloyed gold–silver solutions after irradiation at high dose rate (7.9 MGy h^{-1}) show that isolated and homodisperse clusters of 2–3 nm in diameter are found, thus markedly smaller than at 35 kGy h^{-1} (Fig. 10) [56]. A more sudden and complete reduction of ions into free atoms inhibits not only the intermetal electron transfer, but also, according to the mechanism described for monometallic clusters (Fig. 3a), the process of adsorption/reduction of ions in situ on nuclei (reactions (20)–(21) for mixed clusters), which, in the case of a slow reduction, would instead favor the growth and could not be prevented by the polymer (Fig. 3b).

Likewise, optical absorption studies of bimetallic Au–Pd nanoclusters and local XPS analysis demonstrated the formation of core-shell structures at low irradiation dose rate and, for the first time at room temperature, of alloyed clusters at high dose rate (pulsed EB) [59].

Systems studied are summarized on Table 1. Depending on the rate of the intermetal electron transfer competing with the dose rate-dependent coalescence, alloying:

(i) may occur even at low reduction rate (γ-irradiation with moderate dose rate) [16], as for alloyed Cu_3Pd, CuPd, NiPt, CuAu and AgPt clusters;
(ii) may require higher γ-dose rates [56] as for Ag_xAu_{1-x} (Cl^-) and Ag_xPd_{1-x};
(iii) is only obtained through a short and intense irradiation provided by electron beams [58] as for $Ag_xAu_{1-x}(CN^-)$, AuPd;
(iv) is not obtained even at high dose rate. In spite of the very fast reduction (a few seconds for complete reduction with EB), in some systems the electron transfer was faster and metals are still segregated (Au/Pt, Ag/Cu) [60].

The time-resolved results and the mechanism provided by pulse radiolysis indicate clearly that all metal ions are reducible by the radiolytic strong reductants, but also that they associate readily with atoms and oligomers newly formed as far as the reduction is partial. However, irradiation in the pulse regime cumulates two advantages for the cluster synthesis, one being to penetrate deeply and homogeneously into the system (as in the steady irradiation regime), the second being the capability to produce within a very short time the required equivalents for complete reduction. Obtaining the synthesis of small and alloyed multimetallic clusters depends more on the possibility to inhibit the ion adsorption/reduction on oligomers and the

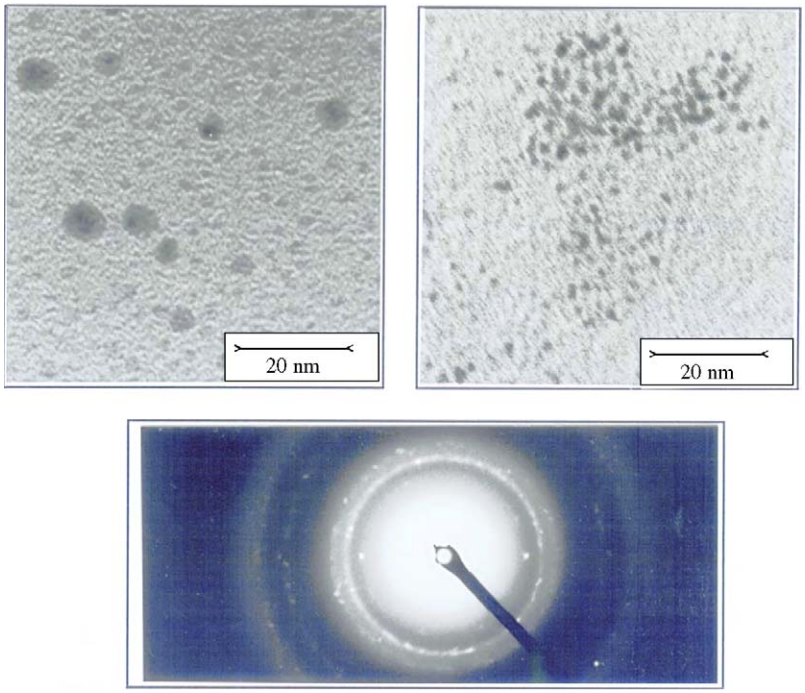

Fig. 10. Micrographs (a and b) and electron diffraction pattern (c) of Ag/Au (50/50) alloyed clusters. (a) Dose rate = 35 kGy h^{-1}, dose = 20 kGy (PA). (b) Dose rate = 7.9 × 10^3 kGy h^{-1}, dose = 30 kGy (PVA). (c) Diffractogram of the sample corresponding to micrograph (a). Note the presence of two central intense spots corresponding to the lattice distance $d_{1\,1\,0}$ due to the existence of a perfectly ordered alloy of A_3B stoichiometry (A = Ag or Au) [56].

intermetallic electron transfer process by this very fast reduction rate, than on the matching between the respective cell parameters of the crystal lattices of the metals. The choice of the dose rate thus offers the means to control the cluster size and the cluster multimetallic structure. The same mechanism, which results from radiolytic experiments, is expected to occur in other reduction methods (by chemical strong reductants or by electro- or photochemically generated radicals), where it can be applied provided the above competitions are taken into account.

5. Application of cluster properties to photography

Metal oligomers and clusters play a major role in silver photography processes [8,61,62]. During the exposure, a few silver atoms only (from 0 to about 10) are produced by the photoelectrons in AgX microcrystals where they form oligomers, but their total amount is too small to vizualize this latent image. The image is revealed due to a further catalytic development of the oligomers by chemical reduction of the surrounding silver cations of the crystal up to black silver grains. This step results in an enormous amplification (×10^7–10^8), together with a specific discrimination preventing from reduction the unexposed parts of the latent image, which are finally dissolved during the fixing step.

5.1. Photographic development mechanism

Though the environment of clusters is different in solutions and at the surface of silver halide crystals embedded in photographic emulsions, we proposed to extend the same growth mechanism (13)–(15), which was demonstrated by pulse radiolysis for clusters Ag_n^+ free in solution, to a theoretical explanation of the development in photography (Fig. 11) [47,61,62]. The development occurs in both cases at the interface between an aqueous solution of an electron donor and a silver cluster acting as an autocatalytic growing site accepting electrons/silver ions. In fact, the various aspects of the catalytic growth revealed by the kinetic studies of solutions [47] mimic the characteristics of the development known experimentally to photographers, in particular the existence of a critical nuclearity as a lower limit for the development, and the dependence of its value on the reduction potential of the developer [8]. According to the mechanism (13)–(15) established in solution [47], the discrimination induced by the developer is explained as the consequence of a quantum-size effect on the silver nuclei redox potential which, at the aqueous interface, does increase with n: the critical nuclearity n_c, as a lower limit, is determined by the threshold imposed by the first one-electron reduction potential of the developer (n_c = 3–5 for usual developers) (Fig. 11). Only supercritical oligomers with a potential higher than that of the developer act as growth nuclei. The model is now widely accepted [63,64]. (Note that the decreasing nuclearity-dependence of the ionizaton potential in the gas phase as shown in Fig. 6 would have resulted in an upper limit, which contradicts the experimental knowledge on development.)

Fig. 11 concerns pure silver clusters as in primary emulsions. However, most of commercial emulsions are sensitized by ions of a more noble metal such as gold. In this case, the nuclearity-dependent potential scale of the initial alloyed clusters, acting further as development nuclei, would be somewhat shifted to more positive values. Thus, it explains that, with a same electron

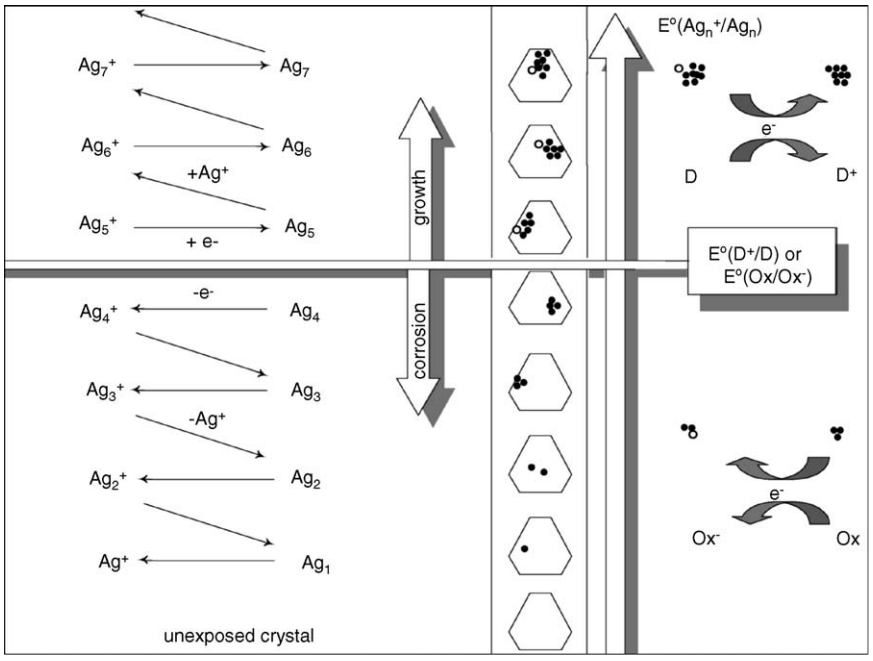

Fig. 11. Photographic development mechanism. The redox potential, $E^{\circ}(Ag_n^+/Ag_n)$, of the latent image clusters, when in contact with a solution, increases with the number of atoms n. Therefore, a nuclearity threshold for development is created by the redox potential of the developer $E^{\circ}(D^+/D)$. Above the critical nuclearity n_c, the potential $E^{\circ}(Ag_n^+/Ag_n)$ is higher than $E^{\circ}(D^+/D)$ and alternate electron transfer toward Ag_n^+ and Ag^+ adsorption on Ag_n let grow the cluster autocatalytically. On the contrary, when $E^{\circ}(Ag_n^+/Ag_n)$ is lower than $E^{\circ}(D^+/D)$, corrosion of subcritical clusters takes place by oxidizing molecules, such as D^+ [47].

donor, the critical nuclearity is lower for gold-sensitized ($n_c = 3$) than for primary emulsions ($n_c = 5$) [51].

5.2. Diffusion transfer processes

Special diffusion transfer processes, such as the photographic offset, require the formation of a silver image at the upper surface and not in the depth of the emulsion. Therefore, after the exposure, the developer dissolves the unexposed crystals of the complementary positive image and let diffuse the silver ions to the emulsion surface, where they are then reduced. In the absence of photonuclei there, some extra germs should be added in the surface layer to induce the reduction-development of this surface image. Metal clusters added as development centers should be small enough to ensure a high resolution and to be active without loss of transparency. Silver nanoclusters produced by γ-irradiation, and particularly alloyed clusters of Ag–Au, Ag–Cu, Ni–Pt and Ag–Cu–Pd prepared under high dose rate conditions exhibit the best activity and resolution [65].

5.3. Enhancement of photographic sensitivity

Another important application to photography of our understanding of the cluster formation mechanism in radiation chemistry is the enhancement of the sensitivity of photographic emulsions [66]. The primary effect of the photon absorption by the silver halide crystals of the emulsion during the exposure is indeed to produce one electron–hole pair per photon absorbed (theoretical quantum yield of unity). However, the effective sensitivity decreases markedly due to the very fast recombination of the initial pairs before electrons reduce silver cations, and to the oxidation by holes of the newly formed atoms (Fig. 12 left). This analogy with $OH^{\bullet}$ oxidation processes occurring in irradiated solutions suggested us to use the same scavenging method to inhibit the electron–hole pair recombination and the oxidation by the holes [66]. When the silver halide crystal has been doped during the precipitation with formate ions ($HCOO^-/Ag^+ = 10^{-6}$), the holes produced during the exposure simultaneously with electrons are indeed immediately scavenged by the formate ions and produce

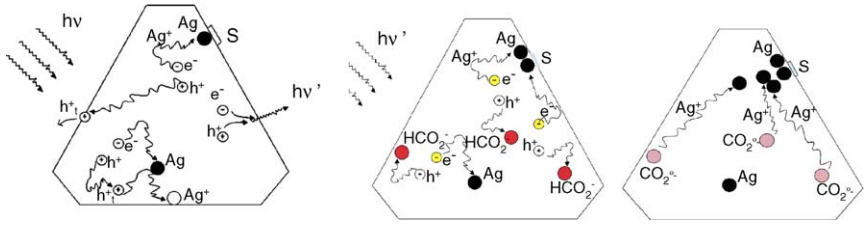

Fig. 12. Photographic latent image formation in undoped and formate-doped and gold-sulfide sensitized AgBr crystals. *Left:* undoped crystal with electron–hole and atom–hole recombination. *Center:* formate-doped crystal and hole scavenging step. *Right:* formate-doped crystal and delayed reduction step of additional silver ions by formyl radical [66].

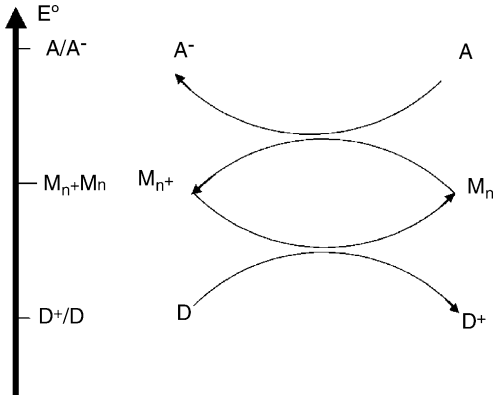

Fig. 13. Scheme of the mechanism of a catalytic electron transfer involving metal clusters as relay. The thermodynamic conditions to be fulfilled are that the cluster redox potential is higher than the donor D and lower than the acceptor A potential. This implies that the cluster is in a size range that offers the efficient redox potential [67].

formyl radicals (an analog to reaction (3); Fig. 12 center). The recombination is suppressed and the yield is enhanced from 0.20 for the undoped reference up to 1 atom per photon for the doped emulsion after immediate developing. The yield is still doubled to an effective quantum yield of 2 atoms per photon when the development is delayed, because a supplementary reduction of Ag^+ by the strong reductant formyl radicals occurs within 15 min (as in reaction (6); Fig. 12 right). This remarkable enhancement is applicable to all processes based on silver imaging, black and white and color photography, radiography and holography [66].

6. Application to catalysis

6.1. Role of cluster properties in catalysis

Actually, one of the important applications of metal clusters is catalysis. A catalytic process generally involves a cascade of repetitive multistep reactions where reactants are transformed into products, and where the catalyst, in spite of its transient interactions with the reactants and products, is steadily regenerated. The catalysts should offer large specific area in order to accelerate the access of reactants to the active sites. Ultra-divided metal clusters are thus particularly efficient in number of reactions. The overall rate of the catalyzed reaction is obviouly controlled by the slowest step of the process.

However, the catalyzed reaction is controlled not only by kinetics, but also by thermodynamics, as in the autocatalyzed growth or development described above (Fig. 11). The thermodynamic aspects concerning the catalyst in the catalyzed reaction are often overlooked, since the elementary reversible mechanism in which the catalyst is implied, possibly at several steps, is generally unknown. Actually, when an overall electron transfer reaction between a donor D and an acceptor A is catalyzed by metal clusters (Fig. 13), they have the capability to play the role of an intermediate electron relay due to their redox properties: in a repetitive cycle, alternatively M_n acts as a donor faced to A, and M_n^+ as an acceptor faced to D [67]. Very small amounts of M_n^+/M_n are thus able to transform large concentrations of D/A into D^+/A^-. This mechanism will reach the optimized efficiency, provided $E^\circ(D^+/D) < E^\circ(M_n^+/M_n) < E^\circ(A/A^-)$ (Fig. 13). This thermodymamical condition also implies that the size of the cluster is small enough to correspond to a potential value in the appropriate range, between two thresholds imposed by D and A. Otherwise, given a system D/A, too a large size cluster (with $E^\circ(A/A^-) < E^\circ(M_n^+/M_n)$), a fortiori a bulk metal, will be unable to transfer the electrons to A, and too a small one (with $E^\circ(M_n^+/M_n) < E^\circ(D^+/D)$), will be irreversibly corroded by transferring electrons to A without receiving the electrons from D. Alloying between two or more metals permits to adjust the potential according to the catalyzed step, or even to successive steps (Section 5.1).

Such electron transfer reactions in solution have been studied by pulse radiolysis and time-correlated absorption spectrophotometry [13,68]. Nanoclusters of metal synthesized by γ-irradiation are so small that the solution does not scatter light and that, for kinetics studies, the clusters can be considered as reactive molecules. The hydrogen production by electron transfer from reduced methylviologen $MV^{\bullet+}$ (as D) to H^+ (as A), which is a reaction with a high activation energy ($MV^{\bullet+}$ is stable though H^+ is present), does not occur unless being catalyzed by metal clusters. It has been much studied as a step of the photoreduction of water, also with clusters prepared by irradiation [69]. The decay rate of $MV^{\bullet+}$ in the presence of gold or platinum clusters [70] is diffusion controlled and first order with respect to the $MV^{\bullet+}$ and cluster concentrations. It is independent of $[H^+]$ as if the surface transfer to H^+ was very fast. Then, the decay is much slower and controlled by H_2 desorption from clusters. It has been demonstrated indeed that electrons donated by reducing radicals can be stored on metal clusters acting as reversible microelectrodes [13]. Similarly, in the disproportionation reaction of the superoxide radical anion $O_2^{\bullet-}$, catalyzed by Pt_n clusters, $O_2^{\bullet-}$ decays first by a protonation at the cluster surface, giving Pt_nHO_2, which then reacts with a second $O_2^{\bullet-}$ to produce O_2 and H_2O_2 [42].

6.2. Radiation-induced supported catalysts

In the following systems, various examples of catalyzed reactions are given under the conditions of their specific application. Radiation-induced clusters exhibit particularly high efficiency and selectivity, assigned to their small and homodisperse size, and possibly to tight bonding to the support.

6.2.1. Iridium clusters supported on Al_2O_3

Alumina-supported iridium clusters are efficient catalysts for hydrazine decomposition in thrusters developed for spacecraft orbit and attitude control systems. To avoid poisoning by oxygen compounds, the synthesis was carried out by irradiation of an iridium solution in liquid ammonia in the presence of the alumina powder [15].

6.2.2. Metal clusters on SnO_2

The radiolytic process has been used to graft metallic nanoaggregates upon SnO_2 transparent counter-electrodes (TCE) in order to improve their electrochemical behaviour

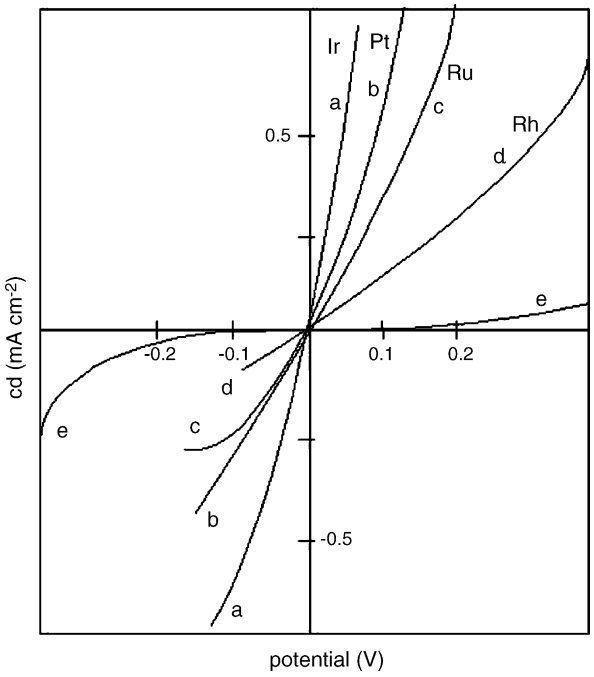

Fig. 14. Current density (cd) vs. voltage curves obtained from unmodified SnO_2 transparent counter electrode (e) or grafted with various metals (a–d) in a 7 M NaI solution. $V = 0$ is the I^-/I_3^- redox potential [45].

[45]. Fig. 14 presents a detectable effect as soon as the concentration of Pt ions in contact with the electrode during the irradiation reaches 10^{-4} mol l^{-1}, and a fairly good electrochemical behaviour with 10^{-3} mol l^{-1} Pt solution. The equivalent thickness has been determined by RBS to be 1 and 3 monolayers, respectively. Among various metals, iridium is shown to give the best catalytic reactivity (Fig. 14). The surface concentration of grafted Ir atoms was found to be around 10^{16} atom cm^{-1}, without any loss of transparency. The electrochemical behaviour of radiolytically grafted TCE is greatly improved, approaching that of the bulk Pt electrode. No decrease in efficiency was observed after 1 month running [45].

6.2.3. Metal clusters on metal electrodes

The radiolytic method was also used to graft metal nanoaggregates upon anodes or cathodes involved in the electrochemical chlorine-soda process [44]. In both cases, important overpotentials are usually measured on unmodified electrodes. Radiation-induced bimetallic nanoparticles (such as Pt–Ru and Ni–Ru), once grafted onto bulk metal electrodes (Ti or Ni), display a remarkable electrocatalytic efficiency. As a synergistic effect, a drastic decreasing of the overpotential is observed when Pt and Ru are alloyed in 2:1 atomic ratio.

6.2.4. Mono and multimetallic clusters supported on carbon

Carbon fibers and powders are used as supports for platinum and alloyed clusters as electrocatalysts for methanol or hydrogen oxidation in fuel cells. Homogeneously dispersed Pt nanoparticles are obtained by irradiation provided the metal is strongly anchored to the carbon surface. These Pt–carbon composites are electroactive in methanol or hydrogen oxidation and in oxygen reduction [36,46]. High loadings have been obtained by the use of CO as ligand for preparing $Pt_x(CO)_y$ clusters which can be loaded on carbon powder up to 60 Pt wt.% while keeping 2–3 nm size. In order to enhance the methanol electrooxidation currents at lower potentials and to extend the catalyst life-time, Pt was alloyed with other metals such as Ru or Sn [12]. Bimetallic Pt–Ru, Pt–Sn and trimetallic Pt–Ru–Sn clusters, stabilized by CO in solution, are prepared by electron beam reduction at high dose rate to enhance the probability of alloying. These clusters are easily impregnated as nanoparticles onto carbon powder at high loading (up to 40 Pt wt.%) without noticeable increase in particle sizes (in the 1–4 nm range). The optimized atomic compositions are $Pt_{0.70}Ru_{0.15}Sn_{0.15}$ and $Pt_{0.70}Ru_{0.20}Sn_{0.10}$ which exhibit a high current density of 650 mA/mg Pt at $0.55V_{SHE}$ (to be compared with pure Pt: 120 mA/mg Pt or with $Pt_{0.70}Ru_{0.30}$: 360 mA/mg Pt, both at $0.55V_{SHE}$). The conclusion on the intimately alloyed character of these bimetallic, a fortiori trimetallic clusters, is deduced from their higher catalytic efficiency, compared to multimetallic clusters synthesized by γ-radiolysis which were found less active, probably because of their core-shell structure (Fig. 14).

6.2.5. Ni clusters on α-alumina or ceria

The temperature-dependence of the methane conversion in the vapo-cracking reaction has been studied over radiolytic catalysts Ni/α-Al_2O_3 (3, 5 and 10 wt.%). The catalytic tests indicate that the reaction starts at low temperature with a very high selectivity (Fig. 15) [18].

When complexed $Ni(NH_3)_6^{2+}$ ions adsorbed on CeO_2 are reduced radiolytically at room temperature, highly dispersed Ni^0 and intermetallic phases NiCe and Ni_2Ce are detected. The catalytic activity in the benzene hydrogenation reaction is remarkably high and the total conversion into cyclohexane is achieved at a particularly low temperature range [19].

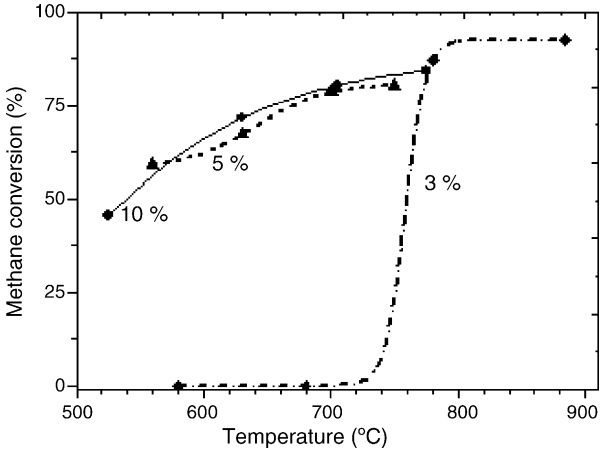

Fig. 15. Temperature-dependence of the methane conversion in the vapo-cracking reaction over the radiolytic catalysts Ni/α-Al_2O_3 at 3, 5 and 10 wt.%. Radiation-induced reduction of Ni^{2+} with a 100 kGy dose at a dose rate of 25 kGy h^{-1}. Catalytic test with a sample of 100 mg. Flow rate of CH_4/H_2O 10% in Ar 1.2 dm^3 h^{-1} [18].

7. Conclusion

Radiation chemistry methods have been proven to be of high potentiality to induce small and size-monodispersed metal clusters, and to study the dynamics of nucleation and growth of clusters, mono and bimetallic, from the monomers to the stable nanoparticle. Their structure, core-shell or alloy, is selected by the dose rate used. Pulse radiolysis provides also the means to observe directly by the time-resolved technique their reactivity, especially to determine during the growth their nuclearity-dependent properties, such as the redox potential. These are of crucial importance for the understanding of the mechanism of the cluster growth itself, in the radiation-induced as well as in the chemical or photochemical reduction process, and also of the mechanism of certain catalytic reactions.

References

[1] W.C. Roentgen, Sitzungs-Ber. Phys-Medizin. Ges. Wuerzburg (1896) 11.
[2] H. Becquerel, C.R. Acad. Sci. 122 (1896) 420.
[3] H. Fricke, J. Chem. Phys. 2 (1934) 556.
[4] M. Haïssinsky, in: J. Dobo, P. Hedwig (Eds.), Radiation Chemistry, vol. 2, Akad. Kiado Buda-pest, 1972, p. 1353.
[5] M. Haïssinsky, La chimie nucléaire et ses applications, Masson & Cie, Paris, 1957.
[6] J.H. Baxendale, E.M. Fielden, J.P. Keene, M. Ebert, in: J.P. Keene, A. Swallow, J.H. Baxendale (Eds.), Pulse Radiolysis, Acadamic Press, London, 1965, p. 207.
[7] M.-O. Delcourt, J. Belloni, Radiochem. Radioanal. Lett. 13 (1973) 329.
[8] J. Bourdon (Ed.), Growth and Properties of Metal Clusters, Studies in Surface Science and Catalysis, vol. 4, Elsevier, Amsterdam, 1980.
[9] N. Basco, S.K. Vidyarthi, D.C. Walker, Can. J. Chem. 51 (1973) 2497.
[10] A. Henglein, Ber. Bunsenges. Phys. Chem. 81 (1977) 556.
[11] J. von Pukies, W. Roebke, A. Henglein, Ber. Bunsenges. Phys. Chem. 72 (1968) 842.
[12] J. Belloni, M. Mostafavi, H. Remita, J.-L. Marignier, M.-O. Delcourt, in: J. Bradley, B. Chaudret (Eds. of the special issue), Synthesis, Chemistry and Some Applications of Metal Nanoparticles, vol. 22, New J. Chem., 1998, p. 1239.
[13] A. Henglein, Chem. Rev. 89 (1989) 1861.
[14] A. Henglein, Ber. Bunsenges. Phys. Chem. 99 (1995) 903.
[15] J. Belloni, M.-O. Delcourt, C. Leclere, Nouv. J. Chim. 6 (1982) 507.
[16] J.-L. Marignier, J. Belloni, M.-O. Delcourt, J.P. Chevalier, Nature 317 (1985) 344;
J. Belloni, J.-L. Marignier, M.-O. Delcourt, M. Minana, US Patent 4,629,709 (1986) and Contn. in part 4,745,094 (1987).
[17] J.-L. Marignier, J. Belloni, J. Chim. Phys. 85 (1988) 21.
[18] N. Keghouche, S. Chettibi, F. Latrèche, M.M. Bettahar, J. Belloni, J.-L. Marignier, Radiat. Phys. Chem. 74 (2005) 185.
[19] S. Chettibi, N. Keghouche, R. Wojcieszak, E.H. Boudjennad, J. Belloni, M. M. Bettahar, Catal. Today 113 (2006) 157–165.
[20] G.V. Buxton, Q.G. Mulazzani, A.B. Ross, J. Phys. Chem. Ref. Data 24 (1995) 1055.
[21] E. Janata, A. Henglein, B.G. Ershov, J. Phys. Chem. 98 (1994) 10888.
[22] M. Mostafavi, S. Remita, M.O. Delcourt, J. Belloni, J. Chim. Phys. 93 (1996) 1828.
[23] J. Belloni, M. Mostafavi, in: C.D. Jonah, M. Rao (Eds.), Studies in Physical and Theoretical Chemistry 87. Radiation Chemistry: Present Status and Future Trends, Elsevier, 2001, p. 411.
[24] M. Mostafavi, G.R. Dey, L. François, J. Belloni, J. Phys. Chem. 106 (2002) 10184;
B. Soroushian, I. Lampre, J. Belloni, M. Mostafavi, Radiat. Phys. Chem. 72 (2005) 111.
[25] G. Mie, Ann. Phys. 25 (1908) 377;
J.A. Creighton, D.J. Eadon, J. Chem. Soc. Faraday Trans. 87 (1991) 3881.
[26] B. Keita, L. Nadjo, H. Remita, J. Belloni, unpublished results.
[27] B. Keita, L. Nadjo, E. Gachard, H. Remita, J. Khatouri, J. Belloni, New J. Chem. 21 (1997) 851.
[28] S. Remita, J.M. Orts, J.M. Feliu, M. Mostafavi, M.-O. Delcourt, Chem. Phys. Lett. 218 (1994) 115.
[29] M. Mostafavi, N. Keghouche, M.-O. Delcourt, J. Belloni, Chem. Phys. Lett. 167 (1990) 193.
[30] B. Keita, L. Nadjo, C. de Cointet, J. Amblard, J. Belloni, Chem. Phys. Lett. 249 (1996) 297.
[31] M. Mostafavi, N. Keghouche, M.-O. Delcourt, Chem. Phys. Lett. 169 (1990) 81.
[32] Lin Ming-Zhang, Thesis, University Paris-Sud, Orsay, 1996.
[33] I. Texier, M. Mostafavi, Radiat. Phys. Chem. 49 (1997) 459.
[34] M.M. Bettahar, M.-O. Delcourt, Radiat. Phys. Chem. 32 (1988) 779.
[35] R. Derai, H. Remita, M.-O. Delcourt, Radiat. Phys. Chem. 38 (1991) 483.
[36] B. Le Gratiet, H. Remita, G. Picq, M.-O. Delcourt, Radiat. Phys. Chem. 47 (1996) 263.
[37] J. Michalik, N. Azuma, J. Sadlo, L. Kevan, J. Phys. Chem. 99 (1995) 4679.
[38] E. Gachard, J. Belloni, M.A. Subramanian, J. Mater. Chem. 6 (1996) 867.
[39] K. Kurihara, J. Kizling, P. Stenius, J.H. Fendler, J. Am. Chem. Soc. 105 (1983) 2574.
[40] J.-L. Marignier, A. Dokuchaev, S. Hautecloque, D. Grand, in: Proceedings of the Seventh International Symposium on Small Part. Inorg. Clusters, 1994, p. 189.
[41] T. Gacoin, F. Chaput, J.P. Boilot, M. Mostafavi, M.-O. Delcourt, in: S. Vilminot, R. Nass, H. Schmidt (Eds.), Eurogel 91 Progress and Development of Processes and Products from Sols and Gels, E-MRS, North Holland, 1991, p. 159.
[42] J. Belloni, M. Lecheheb, Radiat. Phys. Chem. 29 (1987) 89.
[43] J. Amblard, O. Platzer, J. Ridard, J. Belloni, J. Phys. Chem. 96 (1992) 2340.
[44] J. Amblard, J. Belloni, O. Platzer, J. Chim. Phys. 88 (1991) 835.
[45] J. Bruneaux, H. Cachet, M. Froment, J. Amblard, J. Belloni, M. Mostafavi, Electrochim. Acta 32 (1987) 1533.
[46] N. Keghouche, Ph.D. Thesis, Univ. Constantine, 1993.
[47] M. Mostafavi, J.-L. Marignier, J. Amblard, J. Belloni, Radiat. Phys. Chem. 34 (1989) 605.
[48] J. Khatouri, M. Mostafavi, J. Amblard, J. Belloni, Z. Phys. D 26 (1993) 82;
J. Khatouri, M. Mostafavi, J. Ridard, J. Amblard, J. Belloni, Z. Phys. D 34 (1995), 47 and 57.
[49] C. Jackschath, I. Rabin, W. Schulze, Z. Phys. D 22 (1992) 517;
G. Alameddin, J. Hunter, D. Cameron, M.M. Kappes, Chem. Phys. Lett. 192 (1992) 122.
[50] J. Belloni, J. Khatouri, M. Mostafavi, J. Amblard, in: P.J. Rossky, Y. Gauduel (Eds.), Ultrafast Reaction Dynamics and Solvent Effects, vol. 541, Am. Inst. Phys., 1993.
[51] C. de Cointet, M. Mostafavi, J. Khatouri, J. Belloni, J. Phys. Chem. 101 (1997), p. 3512 and 3517.
[52] J. Khatouri, M. Mostafavi, J. Amblard, J. Belloni, Chem. Phys. Lett. 191 (1992) 351.
[53] S. Remita, M. Mostafavi, M.-O. Delcourt, New J. Chem. 18 (1994) 581.
[54] L. François, M. Mostafavi, J. Belloni, J. Delaire, P. Feneyrou, Phys. Chem. Chem. Phys. 3 (2001) 4965.
[55] E. Gachard, H. Remita, J. Khatouri, J. Belloni, B. Keita, L. Nadjo, New J. Chem. 22 (1998) 1257.
[56] M. Treguer, C. de Cointet, H. Remita, J. Khatouri, M. Mostafavi, J. Amblard, J. Belloni, R. De Keyzer, J. Phys. Chem. 102 (1998) 4310.
[57] H. Remita, J. Khatouri, M. Treguer, J. Amblard, J. Belloni, Z. Phys. D. 40 (1997) 127.
[58] A. De Vyt, R. Gijbels, H. Davock, C. Van Roost, I. Geuens, J. Anal. Atom. Spectrom. 14 (1999) 499.
[59] H. Remita, A. Etcheberry, J. Belloni, J. Phys. Chem. B 107 (2003) 31.
[60] S. Remita, G. Picq, J. Khatouri, M. Mostafavi, Radiat. Phys. Chem. 54 (1999) 463.
[61] J. Belloni, in: M. Chanon (Ed.), Homogeneous Photocatalysis, 2, John Wiley, 1997, p. 169.

[62] J. Belloni, in: C. Bréchignac, P. Cahuzac (Eds.), C.R. Ac. Sci., vol. 3, Physique C., 2002, p. 381.
[63] E. Schumacher, Chimia 42 (1988) 357.
[64] J.W. Mitchell, in: M. Sahyun (Ed.), Proceedings of the 48th Annual IS&T Conference on Silver Halides, 1995, p. 136.
[65] Agfa GV Patent no. EP 774690 (1995); no. EP 95203 1706 (1995).
[66] J. Belloni, M. Treguer, H. Remita, R. De Keyzer, Nature 402 (1999) 865; R. De Keyzer, M. Treguer, J. Belloni, H. Remita, US 6,277,549 (August 21, 2001) and Contn in part 6,436,625 (August 20, 2002).
[67] J. Khatouri, M. Mostafavi, J. Belloni, in: J. Wishart, D. Nocera (Eds.), Photochemistry, Radiation Chemistry: Complementary methods for the study of electron transfer, Adv. Chem. Series 54, 1998, p. 293.
[68] J. Belloni, M. Mostafavi, in: P. Braunstein, R. Oro, J. Raithby (Eds.), Metal Clusters in Chemistry, Wiley, VCH, 1999, p. 1213.
[69] D. Meisel, W.A. Mulac, M.S. Matheson, J. Phys. Chem. 85 (1981) 179; M.-O. Delcourt, N. Keghouche, J. Belloni, Nouv. J. Chim. 7 (1983) 131.
[70] E. Amouyal, P. Koffi, J. Photochem. 29 (1985) 277.
[71] P. Mulvaney, M. Giersig, A. Henglein, J. Phys. Chem. 97 (1993) 7061.
[72] A. Henglein, J. Phys. Chem. 96 (1992) 2411.
[73] T. Sosebee, M. Giersig, A. Holzwarth, P. Mulvaney, Ber. Bunsenges. Phys. Chem. 99 (1995) 40.
[74] A. Henglein, P. Mulvaney, A. Holzwarth, T.E. Sosebee, A. Fojtik, Ber. Bunsenges. Phys. Chem. 96 (1992) 754.
[75] M. Michaelis, A. Henglein, P. Mulvaney, J. Phys. Chem. 98 (1994) 6212.
[76] S. Remita, M. Mostafavi, M.-O. Delcourt, Radiat. Phys. Chem. 47 (1996) 275.
[77] Y. Mizukoshi, T. Fujimoto, Y. Nagata, R. Oshima, Y. Maeda, J. Phys. Chem. B 104 (2000) 6028.
[78] P. Mulvaney, M. Giersig, A. Henglein, J. Phys. Chem. 96 (1992) 10419.
[79] F. Henglein, A. Henglein, P. Mulvaney, Ber. Bunsenges. Phys. Chem. 98 (1994) 180.
[80] A. Henglein, M. Giersig, J. Phys. Chem. 98 (1994) 6931.
[81] M. Kumar, S. Kapoor, C. Gopinathan, Radiat. Phys. Chem. 54 (1999) 39.